

Experimental Fluorescence Optical Tomography using Adaptive Finite Elements and Planar Illumination with Modulated Excitation Light

Amit Joshi^a, Wolfgang Bangerth^b, Alan B. Thompson^a, and Eva M. Sevick-Muraca^{a*}

^aThe Photon Migration Laboratory, Texas A&M University, College Station, TX 77843-3573

^bCenter for Subsurface Modeling, Institute for Computational Engineering and Sciences, University of Texas at Austin, Austin, TX 78712

ABSTRACT

Fluorescence enhanced optical tomography is rapidly advancing as a research tool for investigating molecular tissue environments *in vivo* as well as a molecular medical imaging tool. Owing to the scattering nature of near infrared radiation in tissue, iterative tomography approaches must employ the coupled diffusion equations for three-dimensional recovery of fluorescent properties from tissue boundary measurements. Unfortunately, the inverse problem suffers from computational inefficiency and ill-posedness. Furthermore, the resolution attained in fluorescence tomography is limited by a priori fixed discretization of finite element/finite difference schemes used. These difficulties can be ameliorated by employing adaptive discretization strategies. To date, the efficacy of adaptive mesh refinement techniques has yet to be demonstrated in clinically relevant medical imaging situations. In this contribution we present a novel fluorescence tomography scheme which employs dual adaptive finite element meshes for three dimensional reconstructions of fluorescent targets beneath the simulated tissue surface. We demonstrate the tomographic reconstruction from actual experimental data. Frequency domain fluorescence data collected at the illumination surface was used for reconstructing the fluorescence yield distribution in an 8cm x 8cm x 8cm cubical tissue phantom filled with 1% Liposyn solution. Fluorescent targets contained 1 micro-molar Indocyanine Green solution. The tissue phantom was illuminated at the top surface by an expanded 785nm laser modulated at 100 MHz. Fluorescence measurements at the illumination surface were taken by an image intensified CCD camera system outfitted with holographic band rejection and optical band pass filters. Excitation source was quantified by utilizing cross polarizers. Adaptive mesh refinement allows efficient reconstructions for buried fluorescent targets. Image reconstructions for 1cm³ fluorescent target placed at the depth of 1cm from the illumination surface are presented for the perfect and imperfect (100:1) uptake of the fluorescent contrast agent.

Keywords: Optical Tomography, fluorescence imaging, adaptive finite elements, frequency domain.

1. INTRODUCTION

Fluorescence enhanced optical tomography is a promising modality for functional or molecular imaging. It exploits the extended propagation of Near Infrared photons in tissues coupled with molecularly targeting fluorescent probes which excite and emit in NIR region. Fluorescence tomography constructs the map of Fluorophore distribution in the interior of tissue domain from boundary fluorescence measurements obtained with boundary NIR excitation. A unique solution of optical tomography problem requires photon time of flight information¹. Frequency domain mode of optical tomography provides the pertinent photon time of flight information with high signal to noise ratio. The Fluorescence optical tomography systems for clinical applications need to demonstrate rapid data acquisition and computationally efficient and robust image reconstruction capabilities. Herein, we describe a frequency domain fluorescence optical tomography approach which utilizes an area illumination and area detection measurement strategy coupled with an adaptive finite element based image reconstruction algorithm. Area illumination and area detection scheme allows rapid and non-

contact fluorescence measurements and adaptive image reconstruction algorithm provides stable and high resolution three dimensional images of Fluorophore distribution in the tissue phantom.

The outline of this article is as follows: In section 2 we describe the (i) image intensified gain modulated CCD camera based frequency domain fluorescence imaging system, tissue phantom and fluorescent target, (ii) area excitation source characterization, (iii) tomographic reconstruction scheme and (iv) system studies for tomographic reconstruction of fluorescent target in perfect and imperfect conditions. In section 3, we demonstrate tomographic reconstructions for experimental and synthetic measurement data and discuss the enhanced stability and image resolution obtained by employing adaptive finite element based algorithm.

2. MATERIALS AND METHODS

2.1 ICCD homodyne data acquisition system and tissue phantom^{2,3}

Figure-1 presents the ICCD homodyne detection system. The detection system consists of the following major components: (i) a CCD camera (Photometrics Ltd., series AT200, model SI512B, Tucson, AZ), (ii) a gain modulated image intensifier (ITT Industries Night Vision, model FS9910C, Roanoke, VA), (iii) a 785nm laser diode (Thorlabs, HPD 1105-9mm-D-78505) illuminated the tissue phantom, (iv) Oscillators : a PTS-310 frequency synthesizer (Programmed Test Sources Inc., Littleton, MA, model 310M201GYX-53) modulated the photocathode of the image intensifier and a Marconi signal generator (Marconi Instruments Ltd., Hertfordshire, England, model 2022D) modulated the laser diode, (v) Optical filters and lenses: fluorescence measurements are taken with the aid of a 785 nm holographic band rejection filter (Kaiser Optical Systems Inc., Ann Arbor, MI, model HNPf-75.0-2.0) and a 830nm band pass filter (Image Quality, Andover Corp. Salem, NH, model 830.0-2.0), a 50mm Nikkor lens was used to focus the area light signal onto the photocathode of the image intensifier. Frequency domain data was acquired from this system via the homodyne approach wherein the photocathode of the image intensifier and the laser diode were modulated at the same frequency with a variable phase offset, so that the CCD camera captured a steady state image. The phase offset between the oscillators modulating the image intensifier and the laser diode was varied over the full 2π cycle to acquire the complete sinusoid and amplitude and phase associated with the image were then isolated from the fast Fourier transform of the steady state images over the 2π cycle.

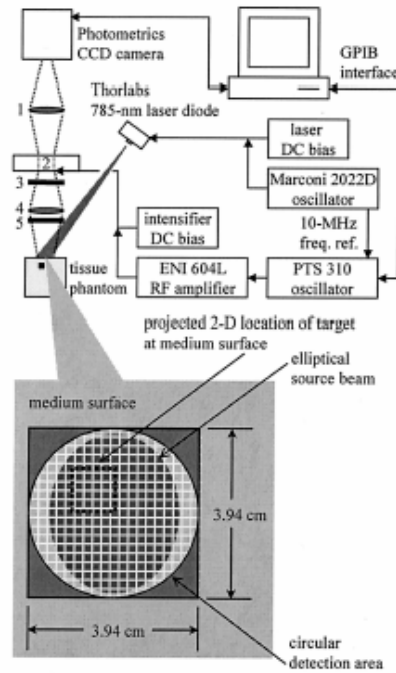


Figure-1: ICCD homodyne system, Numbered components are: 1. 105 mm Nikkor lens, 2. Image intensifier 3. 785nm Holographic band rejection filter, 4. 50 mm Nikkor lens, 5. 830nm band pass interference filter. (Figure reproduced from reference [3])

The tissue phantom was a clear acrylic box with dimensions of 8cm x 8cm x 8cm. It was filled with 1% Liposyn solution (v/v water) (Abbot Labs. North Chicago, IL 60064) to mimic the scattering and absorption properties of human breast tissue. The fluorescent target was a clear 1 cm³ acrylic cube filled with 1 μ M Indocyanine Green (ICG) dye solution in 1% Liposyn. ICG has peak excitation and emission wavelengths of 785nm and 830nm respectively. The target was placed at an off-center position at the depth of 1cm from the illumination surface. Illumination and detection areas were contained within a 3.94cm diameter circular region on the top surface of the tissue phantom. The tissue phantom is illustrated in figure-2. Reduced scattering coefficient in the tissue phantom and target was 10.4 cm⁻¹, absorption due to Liposyn background was 0.023 cm⁻¹ at 785nm and 0.0289cm⁻¹ at 830nm, absorption due to Fluorophore in the target was 0.299cm⁻¹ at 785nm and 0.0506cm⁻¹ at 830nm, Fluorophore lifetime and quantum efficiency were 0.56ns and 0.016 respectively. Figure-3 depicts the fluorescence amplitude and phase images obtained with the ICCD homodyne system. The images are binned down to 128 x 128 bit resolution.

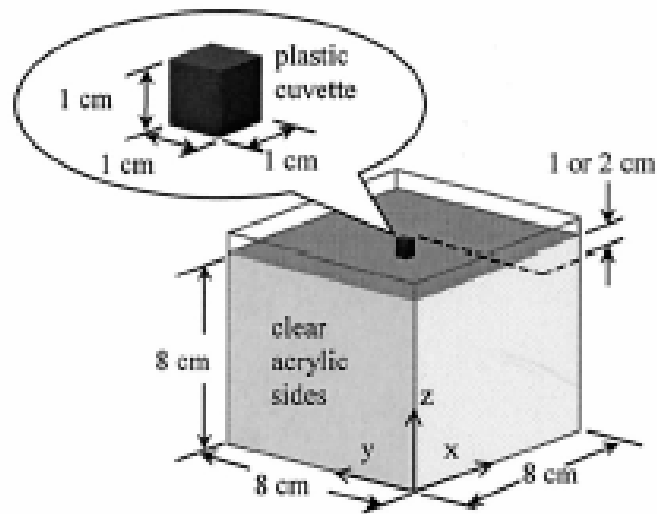


Figure-2: Tissue phantom and target geometry (Figure reproduced from [3])

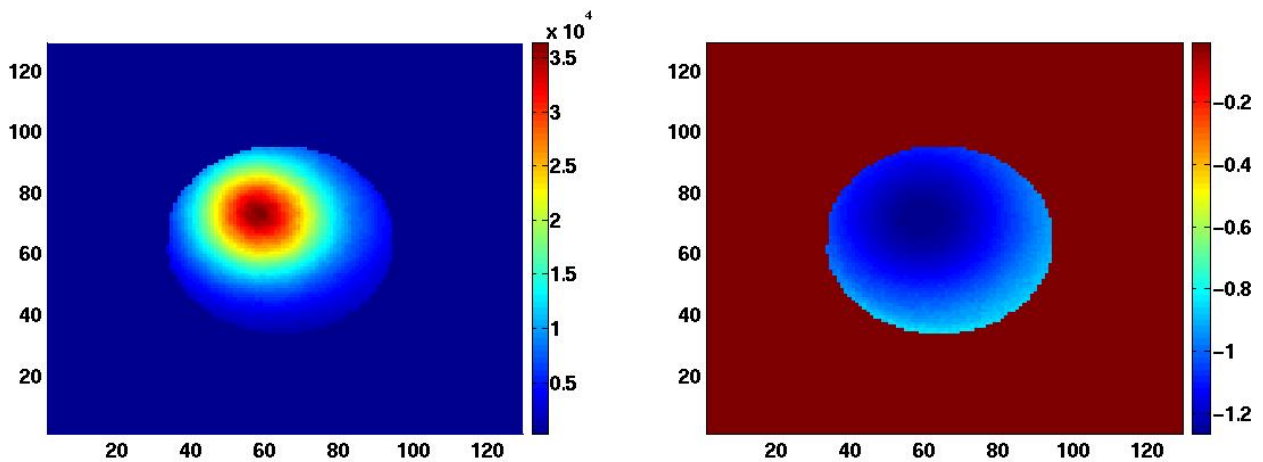


Figure-3: Fluorescence amplitude (left) and phase (right) images acquired for the 1cm³ target suspended 1 cm deep from the illumination surface. Images from the CCD camera are binned down to 128 bit resolution.

2.2 Excitation source characterization³

Model based tomographic reconstruction requires the characterization of expanded laser illumination on the surface of the tissue phantom. A portion of the illumination light is specularly reflected from the phantom surface and it can be taken as the representative of the excitation source amplitude and phase. This specularly reflected light signal was isolated from the diffuse excitation light by employing cross polarizers. Linear polarizers (Newport Corp., model 05P109AR.16, Irvine, CA; Melles Griot, model 03FPI023, Irvine, CA) were positioned at the laser diode output and detector input. Diffuse light becomes randomly polarized due to multiple scattering, while the specularly reflected light retains its polarization. Phase sensitive intensity images were acquired with the polarizer angles aligned parallel and perpendicular to each other for each case. The specularly reflected signal was obtained by subtracting the intensity images obtained with perpendicular orientation of polarization angles of the two polarizers from the intensity images obtained with parallel orientation of the polarizers. The amplitude and phase of the excitation source was obtained from these phase sensitive intensity images by the Homodyne procedure detailed in the previous section. Figure-4 depicts the excitation source amplitude and phase images.

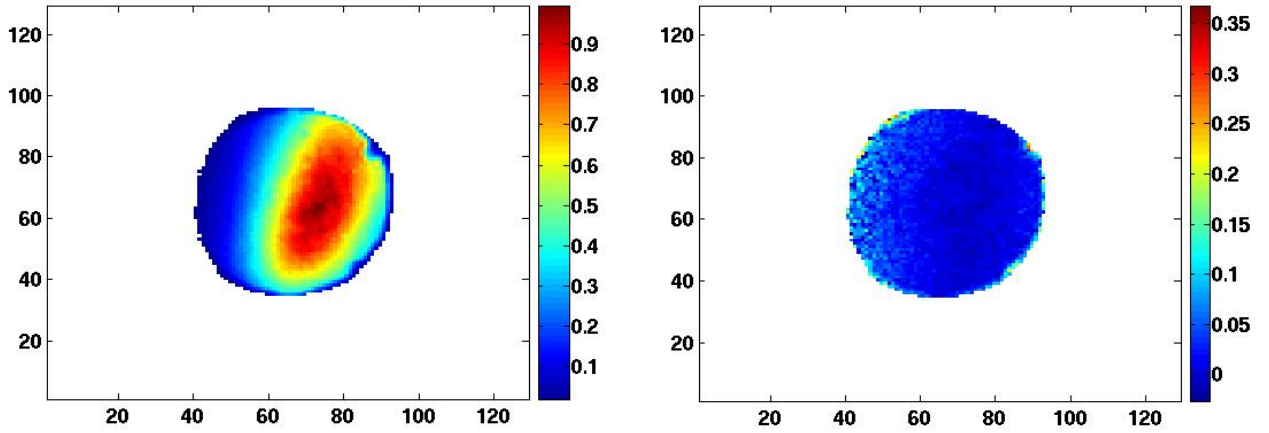


Figure-4: Excitation source amplitude (left) and phase (right)

2.3 Tomography scheme

In fluorescence tomography problem considered in this work, a three dimensional map of absorption due to Fluorophore was reconstructed from the fluorescence amplitude and phase images at the measurement surface of the tissue phantom. Other optical and fluorescence properties were treated as known entities. Image reconstruction was performed by a model based iterative procedure, wherein we solve the following constrained optimization problem⁴:

$$\min_q \frac{1}{2} \|v - \sigma z\|_{\Sigma}^2 + \beta r(q) \text{ subject to photon diffusion model} \quad (1)$$

Here v is the complex fluorescence emission fluence (W/cm^2) predicted from the well known coupled photon diffusion equations⁵; z is the measured fluorescence fluence; σ is the scaling factor accounting for excitation source strength; q is the unknown fluorescence absorption map and $r(q)$ is the Tikhonov regularization functional. This minimization problem is solved with truncated Gauss-Newton method within a Lagrangian formulation to accommodate the constraints imposed by the coupled photon diffusion equations. The solution scheme is describes in detail in reference no [4]. Actual implementation of the reconstruction scheme is on dual adaptive finite element meshes. The coupled diffusion equations are solved on a mesh which gets adaptively refined in locations where excitation and emission fluence shows rapid variation and the parameter map is discretized on a piecewise discontinuous mesh which gets refined in the region of fluorescence target location, as the Gauss-Newton iterations proceed. The actual implementation of the tomography scheme and mesh refinements is not discussed here for lack of space and readers are referred to reference no [4].

2.4 System Studies

Two types of tomography system studies were performed to test the efficacy of the data acquisition system and the image reconstruction algorithm. First study validated the performance of the reconstruction algorithm for synthetic measurement data generated from a 1cm^3 fluorescent target with 100:1 uptake of Fluorophore in the target, for the excitation source detailed in section 2.2 and the measurement configuration and optical properties detailed in section 2.1. Second study focused on performing fluorescence image reconstruction from the experimental fluorescence measurements taken by the ICCD homodyne system and tissue phantom detailed in section 2.1 for perfect uptake of Fluorophore in the tumor.

3. RESULTS AND DISCUSSION

Figure-5 illustrates the tomographic reconstruction from synthetic measurement data for the 100:1 Fluorophore uptake case. The location and size of the target is reconstructed accurately. This underscores the feasibility of tomographic reconstructions from area illumination and area detection measurement configuration. The maximum magnitude of the reconstructed target is 0.144 cm^{-1} which is lower than the actual value of 0.299 cm^{-1} . Figure-6 shows the evolution of forward and inverse meshes during the reconstruction process. The algorithm was started with coarse initial meshes with 64 hexahedral elements. Four automatic mesh refinements were carried out. The final forward mesh consisted of 30269 nodes and was predominantly refined on the illumination plane to resolve the complex structure of excitation source. The final parameter mesh consisted of 1359 elements, mostly located around the reconstructed target. To obtain similar resolution with a uniformly refined mesh, $64^3 (= 262144)$ elements will be required. The advantages of adaptive mesh refinement for the reduction of number of unknowns and improvement of resolution are obvious.

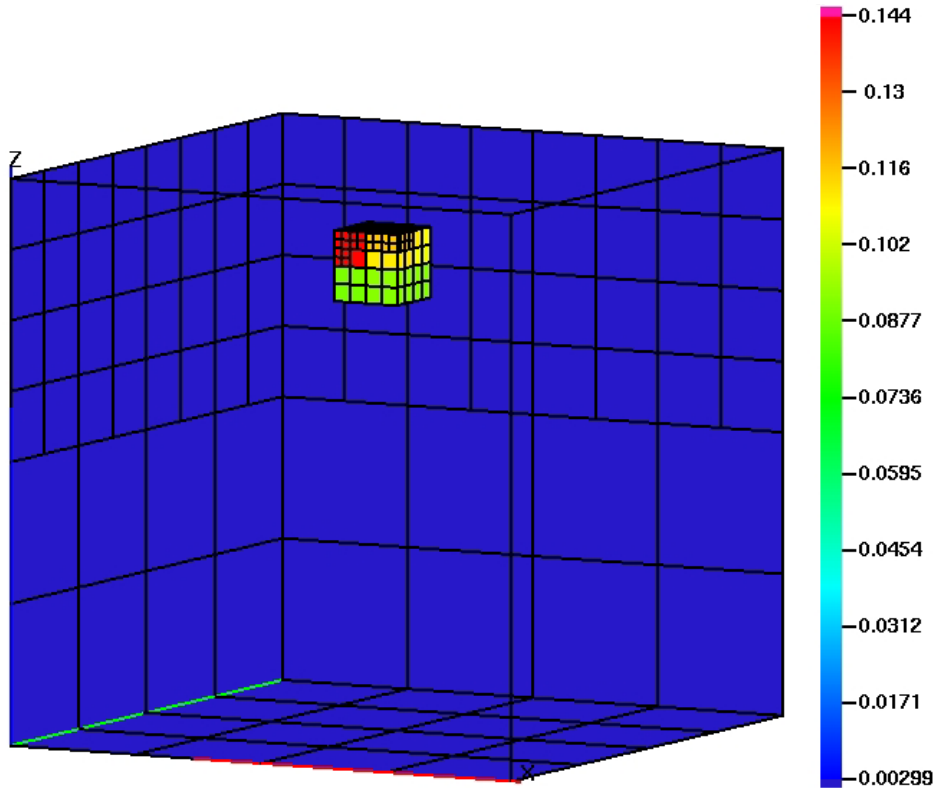


Figure-5: Reconstructed fluorescence absorption distribution from synthetic measurements obtained for 100:1 uptake of ICG in the fluorescent target

Figure-7 illustrates the tomographic reconstruction from measurement data obtained for the perfect Fluorophore uptake case. ICCD fluorescence measurements are corrupted by excitation light leakage and random instrumentation noise, Hence the reconstructed target has correct spatial location, but it is smaller in size and the maximum magnitude of the reconstruction at 1.94cm^{-1} is higher than the actual value of 0.299cm^{-1} .

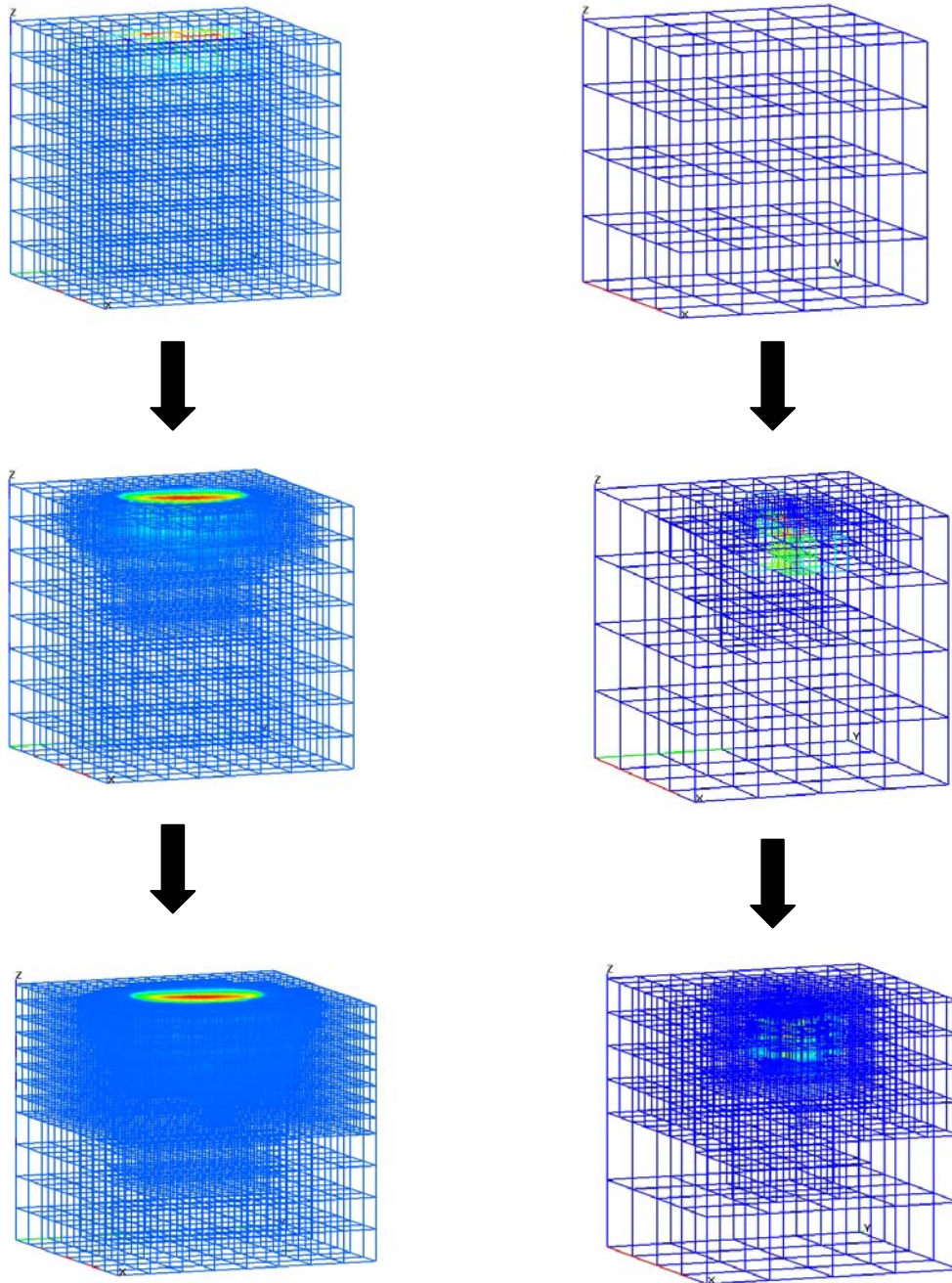


Figure-6: Evolution of forward (left) and parameter (right) meshes. Meshes at 1st, 12th and 26th Gauss-Newton iterations are shown

The final forward mesh contained 10038 nodes and the final parameter mesh consisted of 785 unknowns. The resolution obtained by automatic mesh refinements was one level lower than that for the synthetic measurement data. This might be due to the effect of measurement noise.

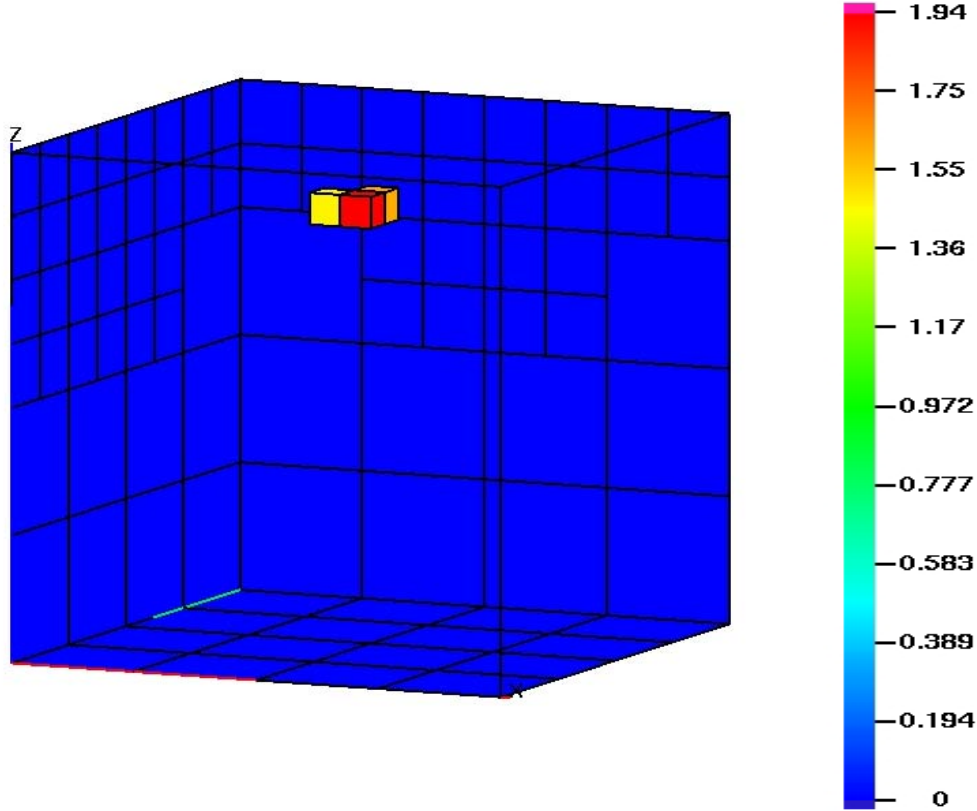


Figure-7 Reconstructed fluorescence absorption map distribution from experimental measurements obtained for perfect uptake of ICG in the fluorescent target

4. CONCLUSION

We have demonstrated an efficient adaptive finite element based scheme for fluorescence optical tomography from non-contact frequency domain fluorescence measurements. The measurements were obtained from an area illumination/area detection ICCD homodyne system. As only the reflectance measurements have been used, this scheme is pertinent for sentinel lymph node mapping as used to track the progress of breast cancer. Our results demonstrate the feasibility of clinical translation of fluorescence tomography as a tool for guiding the surgeon in resection of sentinel lymph nodes by providing depth information⁶. Current and future work is focused towards exploiting adaptive mesh refinement for reconstructing multiple fluorescent targets with varying sizes and separations with data obtained from improved detection systems with enhanced signal to noise ratio and improved excitation light rejection.

ACKNOWLEDGEMENTS

This work was supported in part by NIH R01CA67176.

REFERENCES

1. S. R. Arridge, "Non-uniqueness in diffusion-based optical tomography," *Optics Letters* **23**, 882-884 (1998).
2. A.B.Thompson and E.M.Sevick-Muraca, "NIR fluorescence contrast enhanced imaging with ICCD homodyne detection: measurement precision and accuracy," *Journal of Biomedical Optics* **8**, 111-120 (2002).
3. A.B.Thompson, D.J.Hawrysz, and E.M.Sevick-Muraca, "Near-infrared fluorescence contrast enhanced imaging with area illumination and area detection : the forward imaging problem," *Applied optics* **42**(19), 4125-4136 (2003).
4. A.Joshi, W. Bangerth, and E.M.Sevick-Muraca, "Adaptive finite element based tomography for fluorescence optical imaging in tissue," *Optics Express* **12**(22), 5402 - 5417 (2004).
5. R. Roy and E.M.Sevick-Muraca, "Truncated Newton's optimization scheme for absorption and fluorescence optical tomography: part II reconstruction from synthetic measurements," *Optics Express* **4**(10), 372-382 (1999).
6. S. Kim, Y. T. Lim, E. G. Soltesz, A. M. D. Grand, J. Lee, A. Nakayama, J. A. Parker, T. Mihaljevic, R. G. Laurence, D. M. Dor, L. H. Cohn, M. G. Bawendi, and J. V. Frangioni, "Near-infrared fluorescent type II quantum dots for sentinel lymph node mapping," *Nature Biotechnology* **22**, 93-97 (2004).